

Article

# Synthesis of CBO ( $\text{Co}_3\text{O}_4\text{-Bi}_2\text{O}_3$ ) Heterogeneous Photocatalyst for Degradation of Fipronil and Acetochlor Pesticides in Aqueous Medium

Muhammad Saeed <sup>1,\*</sup> , Sandeep Panchal <sup>2</sup> , Majed A. Bajaber <sup>3</sup> , Ahlam A. Alalwiat <sup>3</sup>, Ahmed Ezzat Ahmed <sup>4,5</sup> , Ujala Razzaq <sup>1</sup>, Hafiza Zahra Rab Nawaz <sup>1</sup> and Farhat Hussain <sup>1</sup>

<sup>1</sup> Department of Chemistry, Government College University Faisalabad, Faisalabad 38000, Pakistan

<sup>2</sup> Department of Civil Engineering, Government Polytechnic Mankeda, Agra 283102, UP, India

<sup>3</sup> Chemistry Department, Faculty of Science, King Khalid University, P.O. Box 9004, Abha 61413, Saudi Arabia

<sup>4</sup> Department of Biology, College of Science, King Khalid University, Abha 61413, Saudi Arabia

<sup>5</sup> Prince Sultan Bin Abdelaziz for Environmental Research and Natural Resources Sustainability Center, King Khalid University, Abha 61421, Saudi Arabia

\* Correspondence: msaeed@gcuf.edu.pk; Tel.: +92-346-9010903

**Abstract:** The excessive use of pesticides has led to the harmful contamination of water reservoirs. Visible-light-driven photocatalysis is one of the suitable methods for the removal of pesticides from water. Herein, the development of CBO ( $\text{Co}_3\text{O}_4\text{-Bi}_2\text{O}_3$ ) as a heterogeneous catalyst for the visible light-assisted degradation of Fipronil and Acetochlor pesticides is reported. After synthesis via coprecipitation using cobalt (II) nitrate hexahydrate ( $\text{Co}(\text{NO}_3)_2 \cdot 6\text{H}_2\text{O}$ ), bismuth (III) nitrate pentahydrate ( $\text{Bi}(\text{NO}_3)_3 \cdot 5\text{H}_2\text{O}$ ) and sodium hydroxide (NaOH) as precursor materials, the prepared CBO was characterized using advanced techniques including XRD, EDS, TEM, SEM, FTIR, and surface area and pore size analysis. Then, it was employed as a photocatalyst for the degradation of Fipronil and Acetochlor pesticides under visible light irradiation. The complete removal of Fipronil and Acetochlor pesticides was observed over CBO photocatalyst using 50 mL (100 mg/L) of each pesticide separately within 120 min of reaction. The reaction kinetics was investigated using a non-linear method of analysis using the Solver add-in. The prepared CBO exhibited a 2.8-fold and 2-fold catalytic performance in the photodegradation of selected pesticides than  $\text{Co}_3\text{O}_4$  and  $\text{Bi}_2\text{O}_3$  did, respectively.

**Keywords:** CBO; pesticides; Fipronil; Acetochlor; photocatalysis



**Citation:** Saeed, M.; Panchal, S.; Bajaber, M.A.; Alalwiat, A.A.; Ahmed, A.E.; Razzaq, U.; Rab Nawaz, H.Z.; Hussain, F. Synthesis of CBO ( $\text{Co}_3\text{O}_4\text{-Bi}_2\text{O}_3$ ) Heterogeneous Photocatalyst for Degradation of Fipronil and Acetochlor Pesticides in Aqueous Medium. *Catalysts* **2024**, *14*, 392. <https://doi.org/10.3390/catal14060392>

Academic Editor: Narendra Kumar

Received: 26 May 2024

Revised: 14 June 2024

Accepted: 17 June 2024

Published: 19 June 2024



**Copyright:** © 2024 by the authors. Licensee MDPI, Basel, Switzerland. This article is an open access article distributed under the terms and conditions of the Creative Commons Attribution (CC BY) license (<https://creativecommons.org/licenses/by/4.0/>).

## 1. Introduction

The intense growth in the human population has led to a significant increase in the demand for food and clean water. Additionally, rapid expansion in industries has accelerated the deterioration of the fresh water supply [1–4]. Various strategies have been adopted for the increase in the production of food. One of the strategies is the employment of agrochemicals called pesticides. Pesticides are agrochemicals commonly employed for the eradication of useless organisms and the preservation of agricultural products. Pesticides are employed for the abatement of pests and weeds to promote the growth of crops and increase the production of food [5,6]. About 2 million tons of pesticides are used annually around the world. However, the excessive use of pesticides causes severe environmental pollution because most of the pesticides disseminate to the environment. It is assumed that less than 15% of the pesticides employed meet their targets [7] (As most of these pesticides are stable and persistent, they therefore remain in soil for a long time. Ultimately, they leach to water bodies as persistent organic pollutants (POPs). Several studies have shown that the toxicological effects of these micropollutants persist even at low concentrations due to their endocrine disruptor potential and become further complicated by their presence as a mixture [8–10]).

Fipronil and Acetochlor are commonly used pesticides in Pakistan. Fipronil, which is generally employed for pest control in veterinary applications, household applications, and agriculture, is a wide-ranging phenylpyrazole insecticide. Its IUPA name is [5-amino-1-[2,6-dichloro-4-(trifluoromethyl) phenyl]-4-[(trifluoromethyl)sulfinyl]-1H-pyrazole-3-carbonitrile] [11]. It is efficacious in the control of insects that have resistance to other insecticides like carbamate, organophosphorus, cyclodiene, and pyrethroids. It disrupts the central nervous system through interfering with the flow of  $\text{Cl}^{1-}$  through the  $\gamma$ -aminobutyric acid-regulated chloride channel [12]. Acetochlor, which is widely used in agriculture applications for the control of annual grasses and broad-leaf weeds, is an effective chloroacetanilide herbicide. Its IPAC name is [2-chloro-N-(ethoxymethyl)-N-(2-ethyl-6-methylphenyl) acetamide] [13,14]. The excessive use of these pesticides causes the contamination of water resources due to water runoff in agricultural fields. Additionally, the industries of pesticide production and domestic wastewater also contribute to the formation of the pesticide-contaminated wastewater. These pesticides are considered as emerging micropollutants. These micropollutants are stable over a long time; therefore, they are transported in water and cause pollution far away from their point source. The existence of these pesticides in surface water and drinking water is a big concern because they are extremely hazardous due to their endocrine disruptor potential. The sporadic use of pesticides has affected ecosystems, which threaten fish, domestic animals, wildlife, birds, and livestock.

Therefore, the treatment of pesticide-contaminated wastewater is a crucial research domain. The conventional methods, including chemical methods (such as electrochemical and chemical precipitation), physical methods (such as adsorption), and biological methods are not effective in the eradication of the pesticide pollutants from the environment. Therefore, advanced methods are needed for the treatment of pesticide-contaminated water [7,15]. Techniques known as advanced oxidation processes (AOPs) are considered effective strategies for the complete remediation of the agrochemicals present in water. These techniques have abilities to mineralize the pesticides to non-toxic inorganic molecules. AOPs comprise various methods including photo-Fenton, Fenton,  $\text{UV}/\text{O}_3$ ,  $\text{O}_3$ ,  $\text{UV}/\text{H}_2\text{O}_2$ , photocatalyst/UV-A, photocatalyst/UV-B, and photocatalyst/Vis. All these methods involve the in situ production of hydroxyl radicals ( $\text{OH}^\bullet$ ) [16–18]. The semiconductor metal oxides-based visible-light-driven photocatalytic method is superior to other methods owing to a low processing cost, the complete decomposition of the pesticide molecules, and mild reaction conditions [19,20]. Only the narrow-band gap semiconductor metal oxides can be employed as visible-light-driven photocatalysts for the degradation of pesticide molecules in the aqueous medium. However, the narrow-band gap semiconductor metal oxides have the drawback of low photocatalytic performance due to the fast recombination of photoinduced charges. Various approaches have been adopted for the improvement of photocatalytic performances of narrow-band gap semiconductor metal oxides. The construction of heterostructure/heterojunction through coupling two or more semiconductor metal oxides is one of the approaches used for the enhancement of photocatalytic performance under visible light irradiation due to its effectiveness and feasibility for the spatial separation of positive holes and electrons [21–23]. The coupling of two semiconductors of different work functions creates a built-in electric field at the interface of the two semiconductors. The creation of a built-in electric field is due to the flow of electrons from the semiconductor having a higher work function compared to the one with a lower work function. As a result, the positive holes accumulate in one component of the heterojunction while the electrons in accumulate other components, and consequently, the recombination is inhibited [24]. The cobalt oxide ( $\text{Co}_3\text{O}_4$ ) and bismuth oxide ( $\text{Bi}_2\text{O}_3$ ) are typical narrow-band semiconductors with a band gap energy of 1.2–2.1 eV and 2.5–2.9 eV, respectively. Although both have a response to the absorption of visible light, they have limited photocatalytic performances due to the quick recombination of positive holes and electrons. The construction of the heterojunction between cobalt oxide ( $\text{Co}_3\text{O}_4$ ) and bismuth oxide ( $\text{Bi}_2\text{O}_3$ ) creates a driving force for the separation of positive holes and elec-

trons. Hence, the construction of a cost-effective CBO ( $\text{Co}_3\text{O}_4\text{-Bi}_2\text{O}_3$ ) composite for the efficient photodegradation of Fipronil and Acetochlor pesticides under sunlight is reported in this study.

## 2. Results and Discussion

### 2.1. Characterization

XRD analysis is a powerful technique to estimate the crystalline nature and crystal structure of the synthesized catalyst. Therefore, the successful synthesis of CBO was confirmed using XRD analysis. Figure 1 shows the XRD spectrum of CBO and standard XRD spectra of  $\text{Co}_3\text{O}_4$  and  $\text{Bi}_2\text{O}_3$ . According to JCPDS No. 42-1476, the diffraction peaks observed in the XRD of CBO at  $2\theta \sim 18, 30, 37, 43,$  and  $58^\circ$  indicate the existence of a cubic structure of  $\text{Co}_3\text{O}_4$  in fabricated CBO. These peaks have been indexed to 111, 200, 311, 200, and 511 planes of the cubic structure of  $\text{Co}_3\text{O}_4$ , respectively [25]. Similarly, the diffraction peaks observed at  $2\theta \sim 19^\circ, 22^\circ, 25^\circ, 26^\circ, 27^\circ, 28^\circ, 33^\circ, 35^\circ, 38^\circ, 46^\circ, 52^\circ, 53^\circ, 54^\circ,$  and  $58^\circ$  correspond to  $\text{Bi}_2\text{O}_3$  according to JCPDS No 41-1449 [26–28]. It can also be observed that the characteristics diffraction peaks of  $\text{Bi}_2\text{O}_3$  in CBO have been slightly shifted. Ding et al. [29] have reported that this slight shift is due to the incorporation of  $\text{Co}^{3+}$ , which has a smaller ion radius (0.063 nm) than  $\text{Bi}^{3+}$  (0.117 nm).

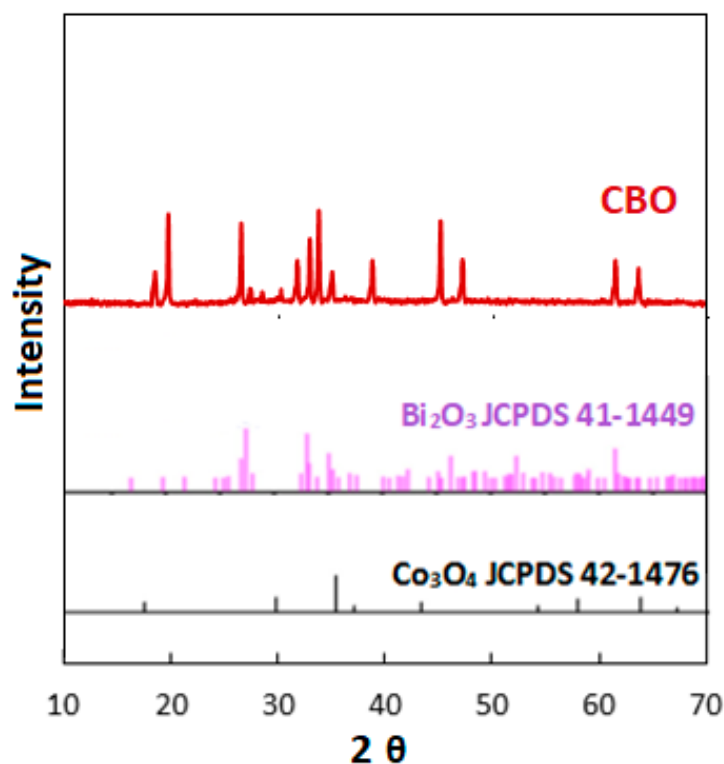


Figure 1. XRD analyses.

Energy dispersive X-ray spectroscopy (EDS) was utilized for the determination of the elemental composition of CBO. The EDS spectrum of CBO is given in Figure 2. The spectroscopic analysis showed that the synthesized heterostructure is composed of cobalt, bismuth, and oxygen. The percentages of these elements are 11.1, 70.8, and 13.9, respectively. The EDS spectrum shows the existence of 4.2% carbon as well in the synthesized CBO. The exact source of this carbon is not known; however, it is considered an impurity in the precursor materials.

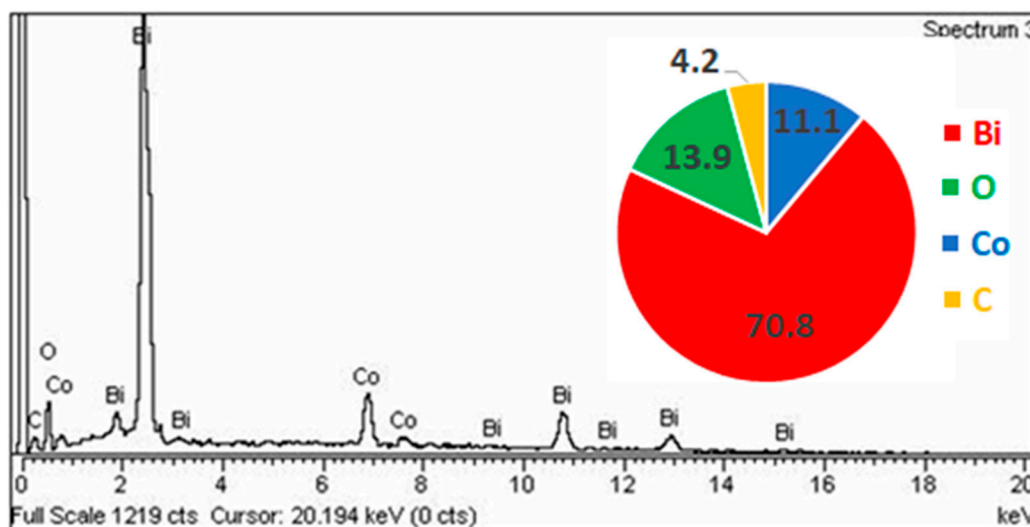


Figure 2. EDS spectrum and percent composition of CBO.

The shape and size of the particles of CBO were studied using TEM and SEM analyses. Figure 3 shows the TEM and SEM images of CBO. TEM indicates that the particle size of CBO is less than 50 nm. The observable lattice fringes in HR-TEM confirm the crystalline nature of CBO. Both the XRD and HR-TEM results support each other. The results of SEM show the dispersed, non-agglomerated, CBO particles and their irregularity in their morphology. The dispersed, non-agglomerated particles have higher catalytic performance because the active centers of such particles are easily accessible to reactant molecules [30]. The TEM image was analyzed for particle size distribution using ImageJ software (<https://imagej.net/ij/>). The particle size distribution is depicted in Figure 3.

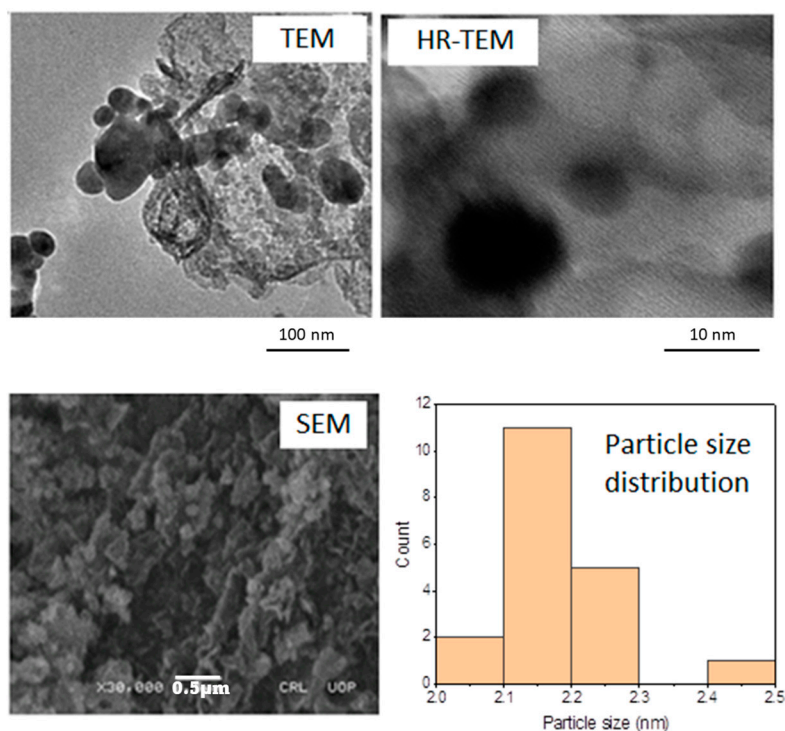


Figure 3. TEM, SEM analyses, and particle size distribution.

The functional groups and bonds associated with synthesized CBO were examined with FTIR spectroscopy. Figure 4 depicts the FTIR spectrum of CBO. Several absorption

bands can be observed in the FTIR spectrum of CBO. The presence of an absorption band at  $1634\text{ cm}^{-1}$  indicates the existence of OH groups on the CBO heterostructure. The existence of Bi-O and Bi-O-Bi linkages can be confirmed using absorption bands at  $\sim 445\text{ cm}^{-1}$  and  $846\text{ cm}^{-1}$ , respectively. The absorption bands at  $\sim 571$  and  $668\text{ cm}^{-1}$  are representative peaks of  $\text{Co}_3\text{O}_4$  due to Co-O stretching vibrations [31–33].

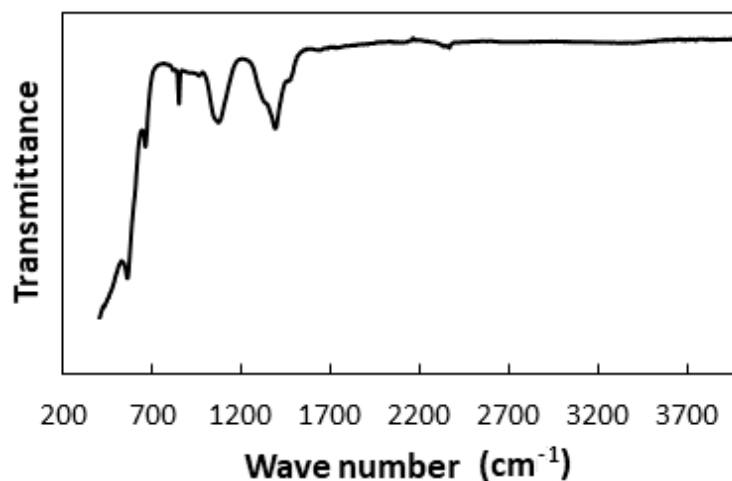


Figure 4. FTIR spectrum of CBO.

The surface area and pore size analyses were carried out by investigating the adsorption of nitrogen at 77.4 K. The surface area calculated through analyzing the nitrogen adsorption data according to the BET equation was found as  $38.53\text{ m}^2/\text{g}$  (Figure 5). Similarly, the pore surface area and pore volume were determined as  $11.13\text{ m}^2/\text{g}$  and  $15.342\text{ cc/g}$  using the BJH method, respectively (Figure 5).

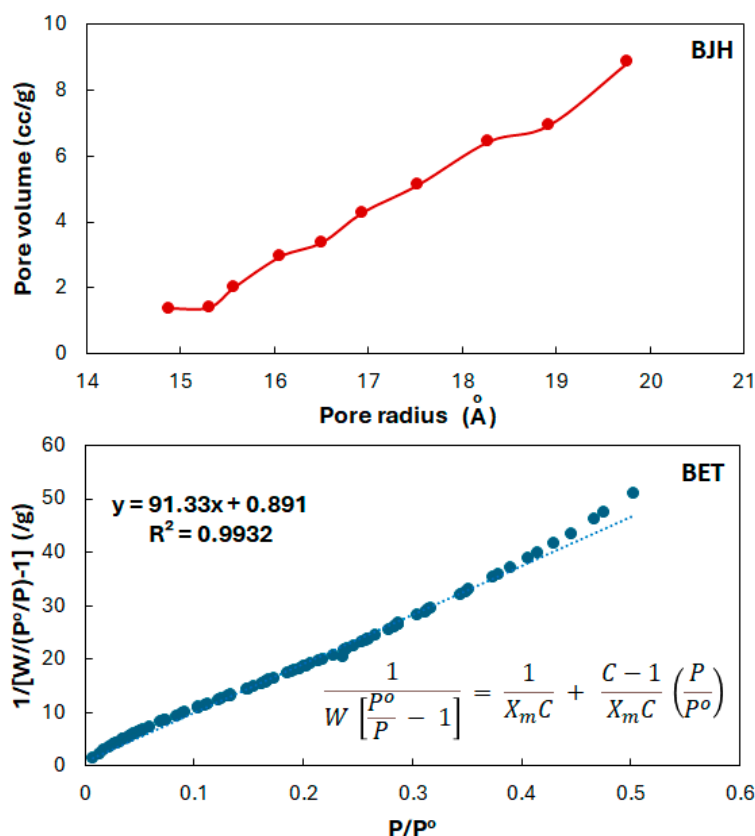


Figure 5. Surface area and pore size analysis.

## 2.2. Photocatalysis

Fipronil and Acetochlor were selected as model pollutants for the evaluation of photocatalytic activities. In the first step, 50 mL of 100 mg/L solution of Fipronil and Acetochlor were stirred under the irradiation of light for 1 h separately. The analysis of the reaction mixture after one hour of stirring showed that there was no loss in the concentration of Fipronil and Acetochlor after stirring the solutions. It confirms that there is no degradation of Fipronil and Acetochlor due to photolysis. In the second step, 0.05 g CBO was added to the solution of Fipronil and Acetochlor in separate experiments. The reaction mixtures were stirred under dark conditions for half an hour. The analyses of reaction mixtures showed about a 20% decrease in the concentration of Fipronil and Acetochlor. This decrease in concentration is attributed to the adsorption of Fipronil and Acetochlor onto the surface of CBO. In the third step, the separate solutions of Fipronil and Acetochlor containing CBO were stirred under sunlight for the evaluation of photocatalytic degradation activities. The analyses showed the complete mineralization of Fipronil and Acetochlor within two hours of the reaction duration. For comparison, the photocatalytic degradation of Fipronil and Acetochlor was carried out with  $\text{Bi}_2\text{O}_3$  and  $\text{Co}_3\text{O}_4$  under similar reaction conditions. More than a 70 and 60% mineralization of Fipronil and Acetochlor were achieved using  $\text{Bi}_2\text{O}_3$  and  $\text{Co}_3\text{O}_4$  as photocatalysts, respectively. Figure 6 depicts the obtained data.

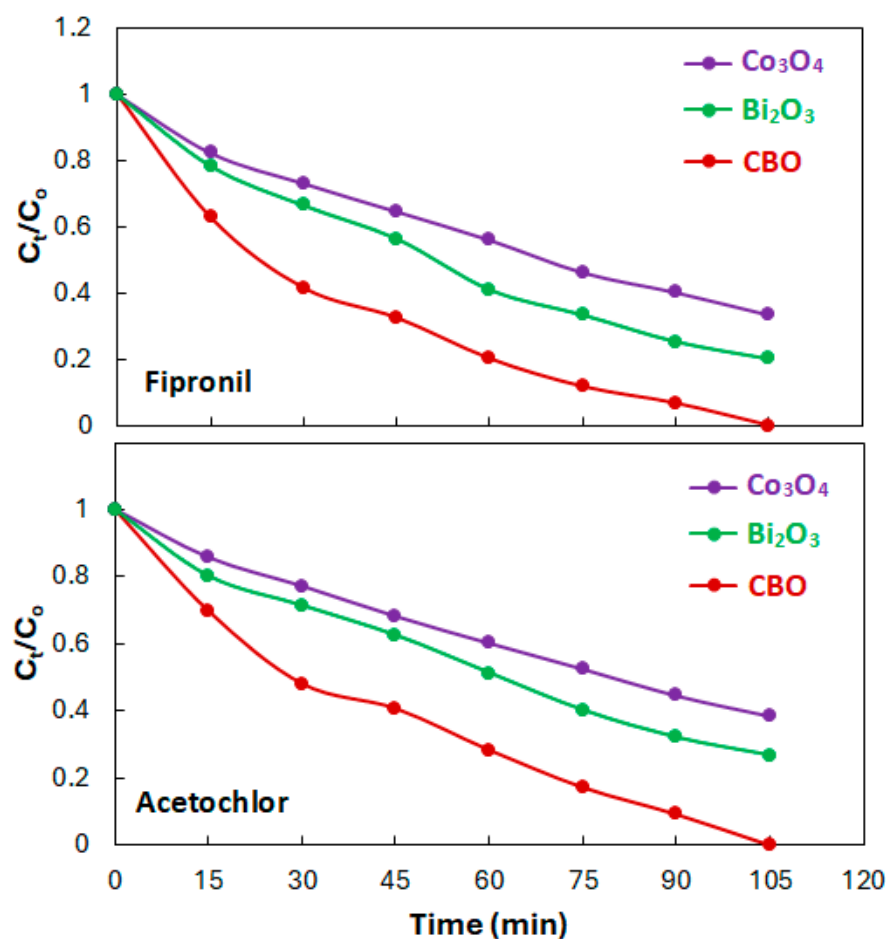
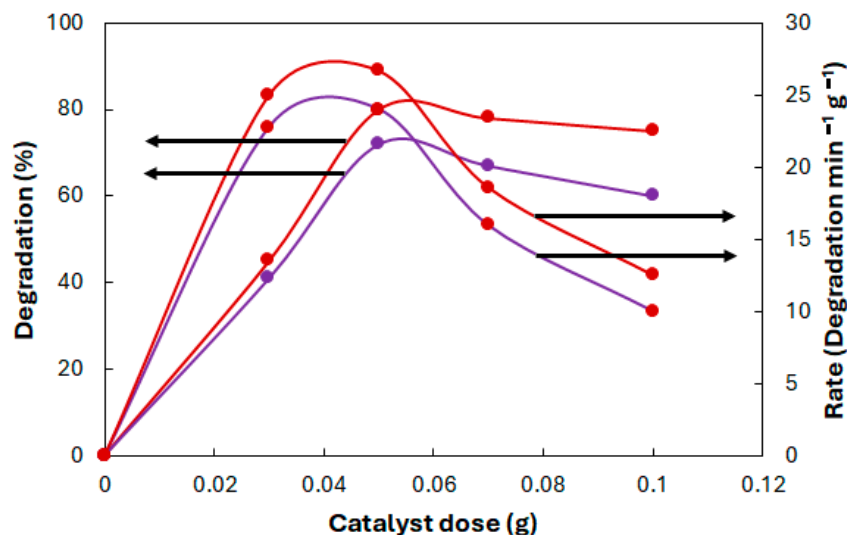


Figure 6. Photocatalytic degradation of Fipronil and Acetochlor.

The optimization of catalyst dose is also an important parameter in catalysis. The use of an optimized catalyst dose avoids the unnecessary utilization of a catalyst in a catalytic reaction. Therefore, the optimum catalyst doses were determined for the photocatalytic degradation of Fipronil and Acetochlor pesticides. This study was accomplished by performing separate photodegradation experiments of Fipronil and Acetochlor with different

dosages of CBO in the range of 0.03 to 0.1 g under the same experimental conditions. Separate 50 mL aqueous solutions of Fipronil and Acetochlor (100 mg/L) were used in this investigation. The reaction duration was 60 min. The obtained results are given in Figure 7. The given data indicate that initially both the percent degradation of Fipronil and Acetochlor and their rate of reaction increased with a catalyst dose from 0.03 to 0.05 g and then a decrease was observed with a higher catalyst dose. Hence, a 0.05 g dose was declared as the optimum catalyst dose in this study. Initially, the catalytic activity increases with the catalyst dose because the number of active centers increases with the catalyst dose. However, the higher catalyst dose causes the scattering of light resulting in a decrease in catalytic activity [3].



**Figure 7.** Effect of catalyst dose on photodegradation of Fipronil and Acetochlor.

The best photocatalyst is one that can be recycled many times without any loss in its photocatalytic activities. Hence, the reusability and stability of the CBO heterogeneous photocatalyst were also studied. The spent CBO samples were collected from the reaction mixture using filtration after photocatalytic degradation experiments. The collected spent sample was first washed many times with ethanol and then with distilled water. After washing, it was dried at 100 °C for 12 h. Then, it was reused as a heterogeneous photocatalyst for the degradation of acetochlor under similar experimental conditions as used earlier. The analyses of samples taken from the reaction mixture showed that the recycled CBO catalyst has almost the same photocatalytic activity as the fresh sample. Hence, it is concluded that fabricated CBO is a stable and reusable heterogeneous photocatalyst for the degradation of pesticides.

### 2.3. Mechanism and Kinetics

The prime reactive species involved in the degradation of selected pesticides were identified through trapping experiments. Separate experiments were performed for the CBO-catalyzed photodegradation of Fipronil in the presence of EDTA and BQ. It was observed that photodegradation of Fipronil decreased from 80% to 68% and 53% in the presence of EDTA and BQ, respectively. The EDTA and BQ have been used as scavengers for  $h^+$  and superoxide anion radicals, respectively. These results confirm that  $h^+$  and superoxide anion radicals are the primary reactive species involved in the degradation of pesticide molecules [34–37]. Hence, the enhanced photocatalytic activity of CBO is attributed to the formation and separation of  $h^+$  and  $e^-$ . As the XRD suggests, synthesized CBO is a mixture of the  $Co_3O_4$ - $Bi_2O_3$  heterojunction and a composite of these two components. Hence, the enhanced photocatalytic activity of synthesized CBO can be explained by two mechanisms.

The CBO is a second-generation photocatalyst. It is also known as a heterojunction. The second-generation photocatalysts were designed to overcome the limitations or

drawbacks associated with first-generation photocatalysts. The fast recombination of positive holes and electrons is the most significant drawback associated with first-generation photocatalysts. In second-generation photocatalysts, these positive holes and electrons are confined to the valence band of one component and the conduction band of other components. Hence, the separation between positive holes and electrons impedes their recombination. Consequently, these species result in the production of highly reactive hydroxyl radicals that take part in the degradation of organic molecules [38,39]. The band edge positions of the components of the CBO heterojunction have been estimated through Mott–Schottky measurement using the theory of electronegativity as reported by Pradhan et al. [40]. Accordingly, the band gap energy, VB, and the CB of  $\text{Co}_3\text{O}_4$ , have been calculated as 2.4 eV, 2.63 eV, and 0.23 eV, respectively. On the other hand, the band gap energy, VB, and CB for  $\text{Bi}_2\text{O}_3$ , have been calculated as 2.7 eV, 2.78 eV, and 0.08 eV, respectively. In a heterojunction, the excited electrons ( $e^-$ ) move from the lower CB of  $\text{Co}_3\text{O}_4$  to the higher CB of  $\text{Bi}_2\text{O}_3$ . The higher CB of  $\text{Bi}_2\text{O}_3$  acts as a barrier to charge recombination. The transfer of  $e^-$  from one component to the other component of heterojunction reduces the recombination of  $h^+$  and  $e^-$ . The separated charges ( $h^+$  and  $e^-$ ) yield hydroxyl radicals in reaction with water and oxygen, respectively. Hydroxyl radicals are powerful oxidizing agents that degrade pollutant molecules [41–43]. Figure 8a explains the possible mechanism.

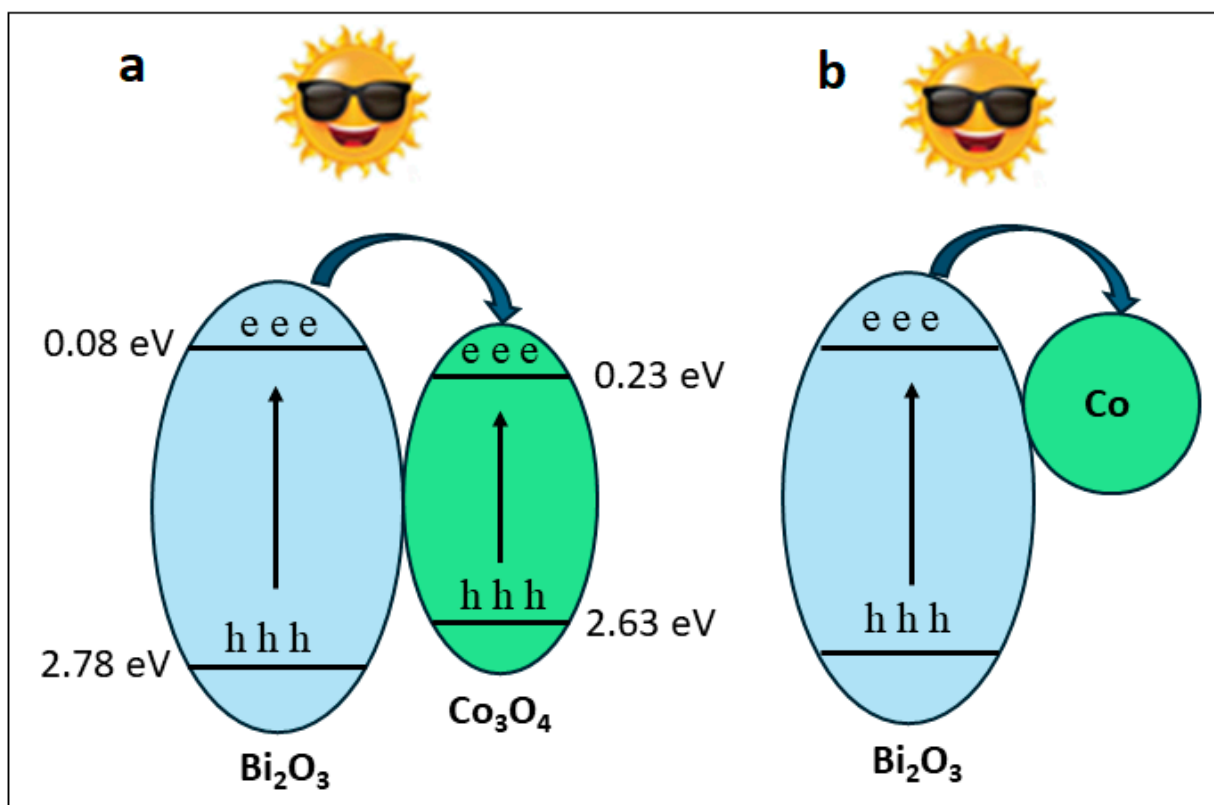
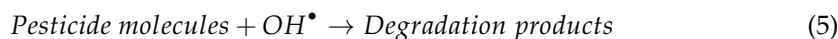


**Figure 8.** Mechanism of photocatalytic process (a) heterojunction (b) doped composite.

The enhanced photocatalytic performance of synthesized CBO can also be explained by another mechanism considering the composite or doped nature of synthesized CBO. As it has been reported in the discussion of XRD analysis, the characteristic diffraction peaks of  $\text{Bi}_2\text{O}_3$  in CBO have been slightly shifted. Ding et al. [29] have reported that this slight shift is due to the incorporation of  $\text{Co}^{3+}$  which has a smaller ion radius (0.063 nm) than  $\text{Bi}^{3+}$  (0.117 nm). The incorporation of  $\text{Co}^{3+}$  in  $\text{Bi}_2\text{O}_3$  acts as a sink for photoexcited electrons and obtains the electrons which restrict the recombination of electrons and holes, resulting in the enhancement of the photocatalytic activity of the CBO [44,45]. Figure 8b explains this mechanism.

The following reactions describe the photocatalytic process:



Based on the above mechanism, the rate of reaction is proposed as ( $h\nu$ : Light energy,  $P$ : Concentration of pesticide)

$$-\frac{dP}{dt} = k(h\nu)(O_2)_{ads}(P) \quad (6)$$

The following experimental conditions make the rate of reaction independent of the first two terms in the above rate expression.

The reaction mixture is continuously irradiated.

The reaction mixture is open to the atmosphere.

Therefore, the rate expression becomes as follows:

$$-\frac{dP}{dt} = k(P) \quad (7)$$

$$-\frac{dP}{P} = k dt \quad (8)$$

$$P = P_0 e^{-kt} \quad (9)$$

where  $P$  and  $P_0$  represent the concentration at a given time and the initial concentration of pesticides in mg/L, respectively. The photocatalytic degradation data of Fipronil and Acetochlor were analyzed according to the kinetic model given in Equation (9) via the non-linear method of analysis using the Solver add-in. Figure 9 shows the analyses of degradation data of Fipronil and Acetochlor via a non-linear method of analysis. The rate constants ( $k$ ) for the degradation of Fipronil and Acetochlor were determined as given in Table 1. The higher values of  $R^2$  indicate the fitness of the kinetics model to experimental data. The observed rate constants show that CBO exhibited 2.8-fold and 2-fold catalytic performance in the photodegradation of selected pesticides than  $Co_3O_4$  and  $Bi_2O_3$ , respectively.

**Table 1.** Rate constants for degradation of Fipronil and Acetochlor.

Catalyst	Fipronil			Acetochlor		
	$k$ ( $\text{min}^{-1}$ )	$R^2$	Half Life (min)	$k$ ( $\text{min}^{-1}$ )	$R^2$	Half Life (min)
$Co_3O_4$	0.0101	0.998	68.6	0.0088	0.999	78.8
$Bi_2O_3$	0.0145	0.997	47.8	0.0119	0.995	58.2
CBO	0.0283	0.997	24.5	0.0233	0.992	29.7

The results of photodegradation of Fipronil and Acetochlor over CBO reported in this study were compared to already reported data as well. For example, Tenri and co-workers [46] have employed 5% AC/Chitosan- $Ca_2Fe_2O_5$  for the photodegradation of Fipronil. They irradiated a 25 mg/L solution of Fipronil containing 0.3 mg/L catalyst for 1 h. They obtained a 77% degradation of Fipronil. Hirashima et al. [47] have investigated the photodegradation of Fipronil using tandem mass spectrometry-liquid

chromatography for the detection of degradation products. They detected many degradation products including dechlorinated compounds. Similarly, Mianjy and Niknafs [48] reported fipronil-desulfinyl as the main degradation product in the photolysis of Fipronil under the irradiation of UV light. Fu et al. [13] studied the  $\text{H}_2\text{O}_2/\text{UV}$ -assisted photocatalytic degradation of acetochlor using  $\alpha\text{-Fe}_2\text{O}_3$  as a catalyst. They investigated the effect of various parameters such as pH, concentration, and  $\alpha\text{-Fe}_2\text{O}_3$  dose on the photocatalytic degradation of acetochlor. The results showed a 91% photocatalytic degradation efficiency with a 50 mg/L solution of acetochlor. Similarly, the  $\text{TiO}_2/\text{UV}$  system has been employed for the successful degradation of metolachlor, acetochlor, and alachlor pesticides in aqueous medium. The maximum degradation efficiency of these pesticides was reported as 98%, 93%, and 97%, respectively. A 1000 mL solution of 10 mg/L concentration was used for each pesticide. Furthermore, the toxicity of these pesticides was also investigated using freshwater alga *Chlorella kessleri* [49]. Wang and co-workers [50] reported the removal of Acetochlor via adsorption and degradation using  $\text{MnFe}_2\text{O}_4@\text{AC}$  as the adsorbent and catalyst. The removal efficiency through adsorption using 0.2 g/L  $\text{MnFe}_2\text{O}_4@\text{AC}$  as the adsorbent was found as 226 mg/g at 25 °C after 10 h of agitation. The removal efficiency of Acetochlor through catalytic degradation was found as >90% through heat-activated peroxy monosulfate (PMS) oxidation. Another research group reported  $\text{BiOBr}$  as a catalyst for the degradation of acetochlor under visible light irradiation. They mainly focused on the dependence of degradation efficiency on catalyst dosage. They found that degradation efficiency increased exponentially with increasing catalyst dosage [51].

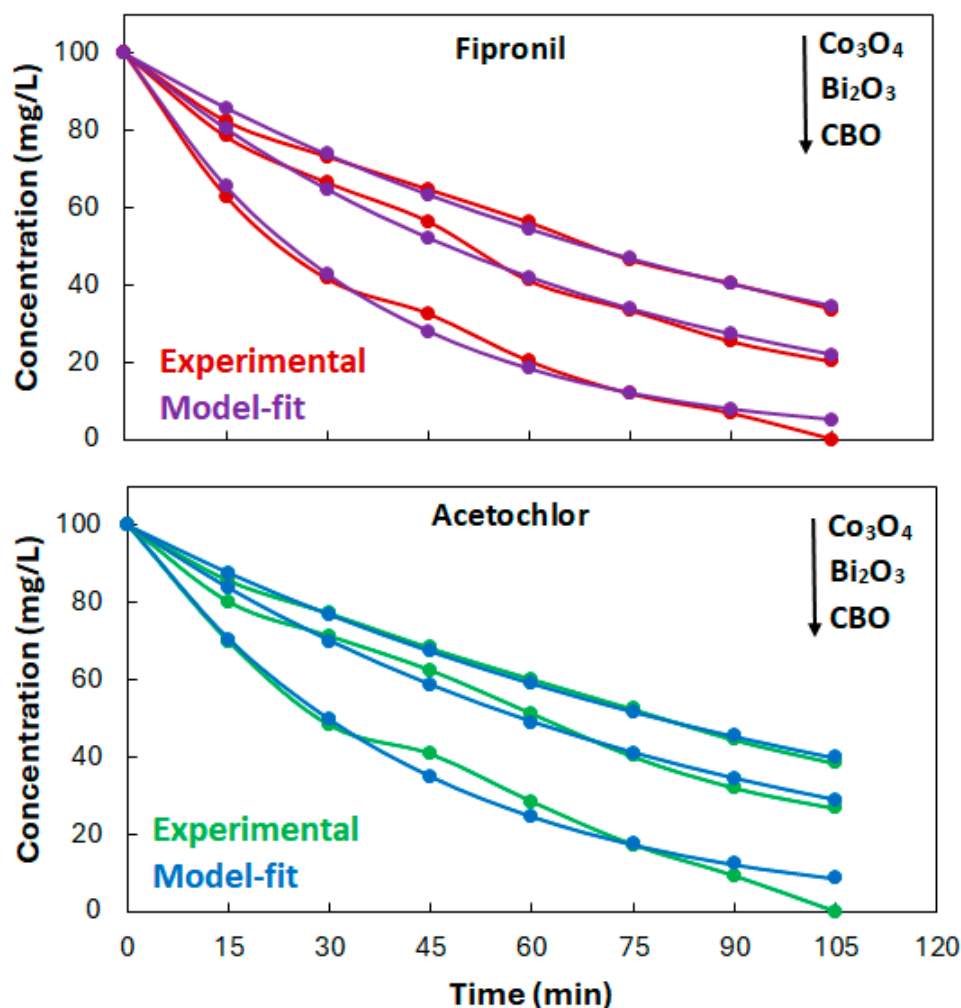


Figure 9. Kinetics analyses.

### 3. Experimental Section

#### 3.1. Synthesis of CBO Heterogeneous Photocatalyst

The photocatalyst CBO was synthesized through the coprecipitation method according to the procedure reported earlier [30]. Typically, a 10 mL solution was prepared by dissolving 10 mmol (2.9 g) cobalt (II) nitrate hexahydrate ( $\text{Co}(\text{NO}_3)_2 \cdot 6\text{H}_2\text{O}$ ) in de-ionized water. Another 10 mL solution was prepared by dissolving 10 mmol (4.85 g) bismuth (III) nitrate in 1 M nitric acid. Then, the solutions of cobalt (II) nitrate hexahydrate and bismuth (III) nitrate were mixed in a beaker. The pH of the resultant mixed solution was adjusted at 12 by dropwise addition of 1 M sodium hydroxide solution from the burette. The resultant mixed solution was continuously stirred for 3 h at a speed of 120 rpm while keeping the temperature constant at 60 °C. As a result of stirring for 3 h, green precipitates of hydroxides of Co and Bi were formed. The resultant precipitates were separated through filtration. The precipitates were washed for the removal of unreacted precursor materials. The washed precipitates were dried at 100 °C for 24 h. Finally, the dried substrate was ground and annealed at 500 °C for 3 h. After cooling to room temperature in the desiccator, the resultant black CBO was ground and sieved via 200 mesh. It was then stored in a glass vial for further study.

#### 3.2. Characterization

The synthesized CBO was characterized by various advanced techniques. Various techniques used for the characterization of CBO include X-ray diffraction spectroscopy, Energy dispersive X-ray spectroscopy, Scanning electron microscopy, Transmission electron microscopy, Infrared spectroscopy and surface area and pore size analysis using JOEL-JDX-3532 (made in Tokyo, Japan), JSM5910 (made in Tokyo, Japan), JEOL-JSM 5910 (made in Tokyo, Japan), JEM 2100 JEOL (made in Tokyo, Japan), and Bruker VRTEX70 (made in Billerica, MA, USA), and NOVA 2200e (made in Connersville, IN, USA), respectively.

#### 3.3. Photocatalysis

The photocatalytic activities of synthesized CBO were explored through the degradation of pesticides Fipronil and Acetochlor, which were selected as model pollutants. The evaluation of photocatalytic activities of CBO was explored in three steps.

A 50 mL solution of Fipronil and/or Acetochlor having a specific concentration was taken in a 500 mL Pyrex glass beaker. The solution of Fipronil and/or Acetochlor was stirred continually under irradiation of ultraviolet or visible light for 1 h. After stirring for one hour, a sample was extracted, and its absorbance was measured. This experiment was performed to know whether Fipronil and Acetochlor degrade under irradiation of ultraviolet or visible light. The analysis showed that there was no degradation of ultraviolet or visible light due to photolysis.

A 0.05 g of CBO was added to the solution of Fipronil and/or Acetochlor after the photolysis experiment. The Fipronil and/or Acetochlor solution containing CBO was stirred continuously under dark conditions for half an hour. After stirring under the dark, a sample was extracted, and its absorbance was measured with a UV-visible spectrophotometer. This experiment was performed to know the removal of Fipronil and Acetochlor due to adsorption on CBO.

The Fipronil and/or Acetochlor solution containing CBO was stirred continuously under irradiation of ultraviolet or visible light. Reaction mixture samples were extracted at different time intervals. The extracted samples were analyzed via measurement of their absorbance values. This experiment was performed to know the removal of Fipronil and Acetochlor due to photocatalytic degradation.

#### 3.4. Analysis of Reaction Mixture

For estimation of photocatalytic activity, the reaction mixture was analyzed via measurement of absorbance of reaction mixture samples extracted at different time intervals at  $\lambda_{\text{max}}$  of Fipronil and Acetochlor. A UV-visible double-beam spectrophotometer (Lambda 25,

Perkin Elmer, Waltham, MA, USA) was used for the analyses of the reaction mixture. For the estimation of photocatalytic degradation of selected pesticides, 10, 15, 20, 25, and 30 mg/L standard solutions of Fipronil and Acetochlor were prepared. The absorbance of each standard solution was measured in the range of 200–250 nm; 350 and 219 nm were found as  $\lambda_{\max}$  of Fipronil and Acetochlor, respectively. The absorbance of each standard solution at  $\lambda_{\max}$  was plotted against concentration. Figure 10 shows these results. The resultant calibration curves were used for the determination of the concentration of Fipronil and Acetochlor in the reaction samples extracted at different time intervals. Then, the following equation was used for the estimation of photocatalytic activity in terms of percent photodegradation of the Fipronil and Acetochlor:

$$\text{Percent degradation} = \frac{C_0 - C}{C_0} \times 100 \quad (10)$$

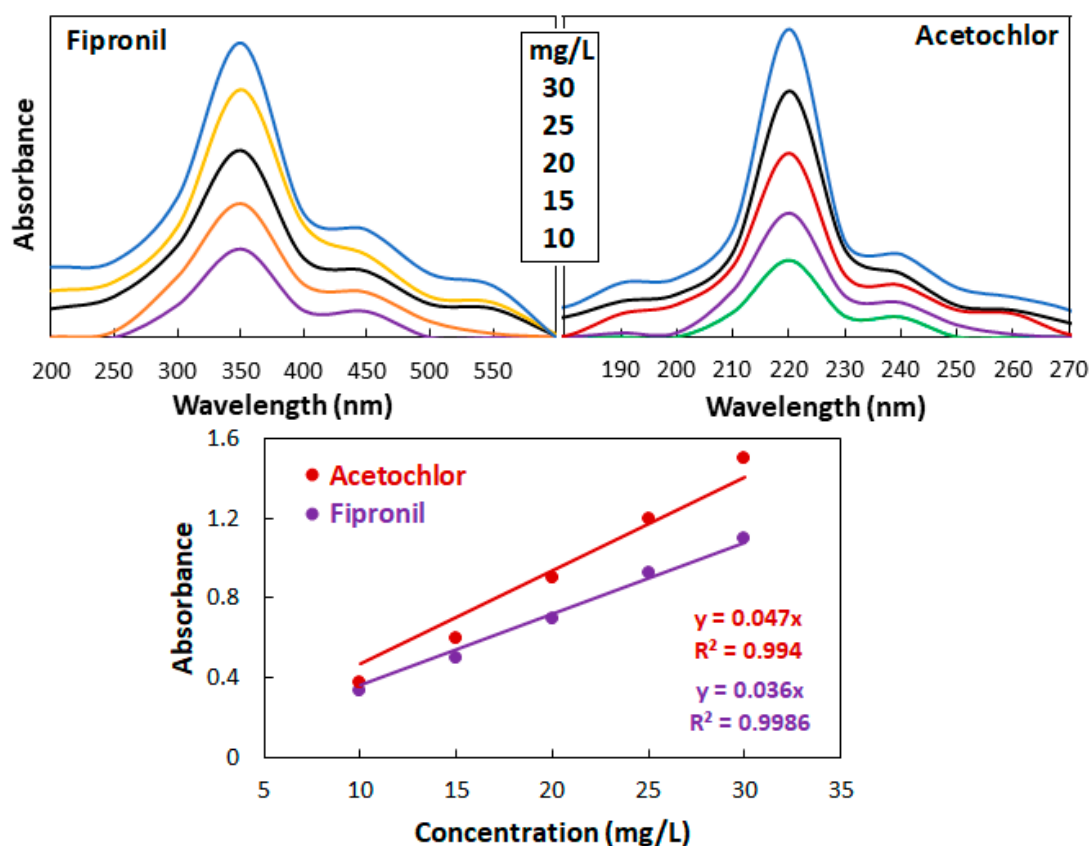


Figure 10. Calibration curves.

#### 4. Conclusions

The photocatalyst CBO was synthesized via coprecipitation using cobalt (II) nitrate hexahydrate, bismuth (III) nitrate, nitric acid, and sodium hydroxide as the precursor materials. The fabrication of  $\text{Co}_3\text{Bi}_2\text{O}_7$  was confirmed with XRD, EDS, TEM, SEM, TGA, FTIR, and surface area analysis. The fabricated  $\text{Co}_3\text{O}_4\text{-Bi}_2\text{O}_3$  was employed as a photocatalyst for the degradation of Fipronil and Acetochlor under visible light irradiation. An almost complete ~75 and ~62% removal of both pesticides was observed with the CBO,  $\text{Bi}_2\text{O}_3$ , and  $\text{Co}_3\text{O}_4$  photocatalysts, respectively. The photodegradation data were analyzed according to a first-order kinetics model using a non-linear method of analysis. The fabricated CBO was found to be an efficient, stable, and reusable photocatalyst for the photodegradation of Fipronil and Acetochlor under visible light irradiation.

**Author Contributions:** Conceptualization, M.S.; methodology, M.S., U.R.; software, S.P.; validation, M.S., and S.P.; formal analysis, M.S., and U.R.; investigation, M.S., U.R., H.Z.R.N., and F.H.; resources, A.E.A.; data curation, M.S.; writing—original draft preparation, M.S.; writing—review and editing, S.P.; visualization, M.S.; supervision, M.S.; project administration, M.S.; funding acquisition, M.A.B. and A.A.A. All authors have read and agreed to the published version of the manuscript.

**Funding:** The authors express their appreciation to the Deanship of Scientific Research at King Khalid University for funding this work through the large group research project under grant number (R.G.P. 2/589/45).

**Data Availability Statement:** Data are contained within the article.

**Acknowledgments:** The authors express their appreciation to the Deanship of Scientific Research at King Khalid University for funding this work through the large group research project under grant number (R.G.P. 2/589/45).

**Conflicts of Interest:** The authors declare no conflicts of interest.

## References

1. Bruckmann, F.S.; Schnorr, C.; Oviedo, L.R.; Knani, S.; Silva, L.F.O.; Silva, W.L.; Dotto, G.L.; Bohn Rhoden, C.R. Adsorption and Photocatalytic Degradation of Pesticides into Nanocomposites: A Review. *Molecules* **2022**, *27*, 6261. [CrossRef]
2. Rout, P.R.; Zhang, T.C.; Bhunia, P.; Surampalli, R.Y. Treatment technologies for emerging contaminants in wastewater treatment plants: A review. *Sci. Total. Environ.* **2021**, *753*, 141990. [CrossRef]
3. Saeed, M.; Akram, N.; Atta-Ul-Haq Naqvi, S.A.R.; Usman, M.; Abbas, M.A.; Adeel, M.; Nisar, A. Green and eco-friendly synthesis of  $\text{Co}_3\text{O}_4$  and  $\text{Ag-Co}_3\text{O}_4$ : Characterization and photo-catalytic activity. *Green Process. Synth.* **2019**, *8*, 382–390. [CrossRef]
4. Younis, S.; Usman, M.; Atta ul Haq Akram, N.; Saeed, M.; Raza, S.; Siddiq, M.; Bukhtawar, F. Solubilization of reactive dyes by mixed micellar system: Synergistic effect of nonionic surfactant on solubilizing power of cationic surfactant. *Chem. Phys. Lett.* **2020**, *738*, 136890. [CrossRef]
5. Lian, L.; Jiang, B.; Xing, Y.; Zhang, N. Identification of photodegradation product of organophosphorus pesticides and elucidation of transformation mechanism under simulated sunlight irradiation. *Ecotoxicol. Environ. Saf.* **2021**, *224*, 112655. [CrossRef]
6. Wang, Z.; Zhang, B.; He, C.; Shi, J.; Wu, M.; Guo, J. Sulfur-based Mixotrophic Vanadium (V) Bio-reduction towards Lower Organic Requirement and Sulfate Accumulation. *Water Res.* **2021**, *189*, 116655. [CrossRef]
7. Yeganeh, M.; Charkhloo, E.; Sobhi, H.R.; Esrafil, A.; Gholami, M. Photocatalytic processes associated with degradation of pesticides in aqueous solutions: Systematic review and meta-analysis. *Chem. Eng. J.* **2022**, *428*, 130081. [CrossRef]
8. Ferhi, S.; Vieillard, J.; Garau, C.; Poultier, O.; Demey, L.; Beaulieu, R.; Penalva, P.; Gobert, V.; Portet-Koltalo, F. Pilot-scale direct UV-C photodegradation of pesticides in groundwater and recycled wastewater for agricultural use. *J. Environ. Chem. Eng.* **2021**, *9*, 106120. [CrossRef]
9. González, V.J.; Vázquez, E.; Villajos, B.; Tolosana-Moranchel, A.; Duran-Valle, C.; Faraldos, M.; Bahamonde, A. Eco-friendly mechanochemical synthesis of titania-graphene nanocomposites for pesticide photodegradation. *Sep. Purif. Technol.* **2022**, *289*, 120638. [CrossRef]
10. Luna-Sanguino, G.; Ruíz-Delgado, A.; Duran-Valle, C.J.; Malato, S.; Faraldos, M.; Bahamonde, A. Impact of water matrix and oxidant agent on the solar assisted photodegradation of a complex mix of pesticides over titania-reduced graphene oxide nanocomposites. *Catal. Today* **2021**, *380*, 114–124. [CrossRef]
11. Gomes Júnior, O.; Borges Neto, W.; Machado, A.E.H.; Daniel, D.; Trovó, A.G. Optimization of fipronil degradation by heterogeneous photocatalysis: Identification of transformation products and toxicity assessment. *Water Res.* **2017**, *110*, 133–140. [CrossRef]
12. de Lima, O.J.; de Araújo, D.T.; Marçal, L.; Crotti, A.E.M.; Machado, G.S.; Nakagaki, S.; de Faria, E.H.; Ciuffi, K.J. Photodegradation of Fipronil by Zn- $\text{AlPO}_4$  Materials Synthesized by Non-Hydrolytic Sol-Gel Method. *Chemengineering* **2022**, *6*, 55. [CrossRef]
13. Fu, Y.; Li, Y.; Hu, J.; Li, S.; Qin, G. Photocatalytic degradation of acetochlor by  $\alpha\text{-Fe}_2\text{O}_3$  nanoparticles with different morphologies in aqueous solution system. *Optik* **2019**, *178*, 36–44. [CrossRef]
14. Li, H.; Wang, Y.; Fu, J.; Hu, S.; Qu, J. Degradation of acetochlor and beneficial effect of phosphate-solubilizing *Bacillus* sp. ACD-9 on maize seedlings. *3 Biotech* **2020**, *10*, 67. [CrossRef]
15. Bokhari, T.H.; Ahmad, N.; Jilani, M.I.; Saeed, M.; Usman, M.; Haq, A.U.; Rehman, R.; Iqbal, M.; Nazir, A.; Javed, T. UV/ $\text{H}_2\text{O}_2$ , UV/ $\text{H}_2\text{O}_2$ / $\text{SnO}_2$  and Fe/ $\text{H}_2\text{O}_2$  based advanced oxidation processes for the degradation of disperse violet 63 in aqueous medium. *Mater. Res. Express* **2020**, *7*, 015531. [CrossRef]
16. Dewil, R.; Mantzavinos, D.; Poullos, I.; Rodrigo, M.A. New perspectives for Advanced Oxidation Processes. *J. Environ. Manag.* **2017**, *195*, 93–99. [CrossRef]
17. Miklos, D.B.; Remy, C.; Jekel, M.; Linden, K.G.; Drewes, J.E.; Hübner, U. Evaluation of advanced oxidation processes for water and wastewater treatment—A critical review. *Water Res.* **2018**, *139*, 118–131. [CrossRef]
18. Ribeiro, A.R.; Nunes, O.C.; Pereira, M.F.R.; Silva, A.M.T. An overview on the advanced oxidation processes applied for the treatment of water pollutants defined in the recently launched Directive 2013/39/EU. *Environ. Int.* **2015**, *75*, 33–51. [CrossRef]

19. Xue, Y.; Liu, X.; Zhang, N.; Shao, Y.; Xu, C.C. Enhanced photocatalytic performance of iron oxides@HTCC fabricated from zinc extraction tailings for methylene blue degradation: Investigation of the photocatalytic mechanism. *Int. J. Miner. Met. Mater.* **2023**, *30*, 2364–2374. [[CrossRef](#)]
20. Yu, F.; Li, C.; Li, W.; Yu, Z.; Xu, Z.; Liu, Y.; Wang, B.; Na, B.; Qiu, J. II-Skeleton Tailoring of Olefin-Linked Covalent Organic Frameworks Achieving Low Exciton Binding Energy for Photo-Enhanced Uranium Extraction from Seawater. *Adv. Funct. Mater.* **2024**, *34*, 2307230. [[CrossRef](#)]
21. Li, R.; Gao, T.; Wang Yao Chen, Y.; Luo, W.; Wu, Y.; Xie, Y.; Wang Yong Zhang, Y. Engineering of bimetallic Au–Pd alloyed particles on nitrogen defects riched g-C<sub>3</sub>N<sub>4</sub> for efficient photocatalytic hydrogen production. *Int. J. Hydrogen Energy* **2024**, *63*, 1116–1127. [[CrossRef](#)]
22. Liu, Y.; Liu, N.; Lin, M.; Huang, C.; Lei, Z.; Cao, H.; Qi, F.; Ouyang, X.; Zhou, Y. Efficient visible-light-driven S-scheme AgVO<sub>3</sub>/Ag<sub>2</sub>S heterojunction photocatalyst for boosting degradation of organic pollutants. *Environ. Pollut.* **2023**, *325*, 121436. [[CrossRef](#)]
23. Soni, V.; Sonu Sudhaik, A.; Singh, P.; Thakur, S.; Ahamad, T.; Nguyen, V.H.; Thi, L.A.P.; Quang, H.H.P.; Chaudhary, V.; Raizada, P.; et al. Visible-light-driven photodegradation of methylene blue and doxycycline hydrochloride by waste-based S-scheme heterojunction photocatalyst Bi<sub>5</sub>O<sub>7</sub>I/PCN/tea waste biochar. *Chemosphere* **2024**, *347*, 140694. [[CrossRef](#)]
24. Yang, H. A short review on heterojunction photocatalysts: Carrier transfer behavior and photocatalytic mechanisms. *Mater. Res. Bull.* **2021**, *142*, 111406. [[CrossRef](#)]
25. Malefane, M.E. Co<sub>3</sub>O<sub>4</sub>/Bi<sub>4</sub>O<sub>5</sub>I<sub>2</sub>/Bi<sub>5</sub>O<sub>7</sub>I C-scheme heterojunction for degradation of organic pollutants by light-emitting diode irradiation. *ACS Omega* **2020**, *5*, 26829–26844. [[CrossRef](#)]
26. Yasin, M.; Saeed, M.; Muneer, M.; Usman, M.; ul Haq, A.; Sadia, M.; Altaf, M. Development of Bi<sub>2</sub>O<sub>3</sub>-ZnO heterostructure for enhanced photodegradation of rhodamine B and reactive yellow dyes. *Surf. Interfaces* **2022**, *30*, 101846. [[CrossRef](#)]
27. Yi, S.; Yue, X.; Xu, D.; Liu, Z.; Zhao, F.; Wang, D.; Lin, Y. Study on photogenerated charge transfer properties and enhanced visible-light photocatalytic activity of p-type Bi<sub>2</sub>O<sub>3</sub>/n-type ZnO heterojunctions. *New J. Chem.* **2015**, *39*, 2917–2924. [[CrossRef](#)]
28. Hu, L.; Zhang, G.; Liu, M.; Wang, Q.; Dong, S.; Wang, P. Application of nickel foam-supported Co<sub>3</sub>O<sub>4</sub>-Bi<sub>2</sub>O<sub>3</sub> as a heterogeneous catalyst for BPA removal by peroxymonosulfate activation. *Sci. Total. Environ.* **2019**, *647*, 352–361. [[CrossRef](#)]
29. Ding, Y.; Zhu, L.; Huang, A.; Zhao, X.; Zhang, X.; Tang, H. A heterogeneous Co<sub>3</sub>O<sub>4</sub>-Bi<sub>2</sub>O<sub>3</sub> composite catalyst for oxidative degradation of organic pollutants in the presence of peroxymonosulfate. *Catal. Sci. Technol.* **2012**, *2*, 1977–1984. [[CrossRef](#)]
30. Saeed, M.; Alwadai, N.; Ben Farhat, L.; Baig, A.; Nabgan, W.; Iqbal, M. Co<sub>3</sub>O<sub>4</sub>-Bi<sub>2</sub>O<sub>3</sub> heterojunction: An effective photocatalyst for photodegradation of rhodamine B dye. *Arab. J. Chem.* **2022**, *15*, 103732. [[CrossRef](#)]
31. Hammad, A.H.; Marzouk, M.A.; ElBatal, H.A. The Effects of Bi<sub>2</sub>O<sub>3</sub> on Optical, FTIR and Thermal Properties of SrO-B<sub>2</sub>O<sub>3</sub> Glasses. *Silicon* **2016**, *8*, 123–131. [[CrossRef](#)]
32. Li, R.; Zhou, D.; Luo, J.; Xu, W.; Li, J.; Li, S.; Cheng, P.; Yuan, D. The urchin-like sphere arrays Co<sub>3</sub>O<sub>4</sub> as a bifunctional catalyst for hydrogen evolution reaction and oxygen evolution reaction. *J. Power Sources* **2017**, *341*, 250–256. [[CrossRef](#)]
33. Tang, X.; Feng, Q.; Huang, J.; Liu, K.; Luo, X.; Peng, Q. Carbon-coated cobalt oxide porous spheres with improved kinetics and good structural stability for long-life lithium-ion batteries. *J. Colloid Interface Sci.* **2018**, *510*, 368–375. [[CrossRef](#)]
34. Khan, I.; Luo, M.; Guo, L.; Khan, S.; Wang, C.; Khan, A.; Saeed, M.; Zaman, S.; Qi, K.; Liu, Q.L. Enhanced visible-light photoactivities of porous LaFeO<sub>3</sub> by synchronously doping Ni<sup>2+</sup> and coupling TS-1 for CO<sub>2</sub> reduction and 2,4,6-trinitrophenol degradation. *Catal. Sci. Technol.* **2021**, *11*, 6793–6803. [[CrossRef](#)]
35. Khan, I.; Luo, M.; Khan Sohail Asghar, H.; Saeed, M.; Khan Shoab Khan, A.; Humayun, M.; Guo, L.; Shi, B. Green synthesis of SrO bridged LaFeO<sub>3</sub>/g-C<sub>3</sub>N<sub>4</sub> nanocomposites for CO<sub>2</sub> conversion and bisphenol A degradation with new insights into mechanism. *Environ. Res.* **2022**, *207*, 112650. [[CrossRef](#)]
36. Saeed, M.; Khan, I.; Adeel, M.; Akram, N.; Muneer, M. Synthesis of a CoO-ZnO photocatalyst for enhanced visible-light assisted photodegradation of methylene blue. *New J. Chem.* **2022**, *46*, 2224–2231. [[CrossRef](#)]
37. Wan, Q.; Liu, R.X.; Zhang, Z.; Wu, X.D.; Hou, Z.W.; Wang, L. Recent Advances in the Electrochemical Defluorinative Transformations of C–F Bonds. *Chin. J. Chem.* **2024**. [[CrossRef](#)]
38. Yang, L.; Li, Z.; Wang, X.; Li, L.; Chen, Z. Facile electrospinning synthesis of S-scheme heterojunction CoTiO<sub>3</sub>/g-C<sub>3</sub>N<sub>4</sub> nanofiber with enhanced visible light photocatalytic activity. *Chin. J. Catal.* **2024**, *59*, 237–249. [[CrossRef](#)]
39. Zheng, Y.; Liu, Y.; Guo, X.; Chen, Z.; Zhang, W.; Wang, Y.; Tang, X.; Zhang, Y.; Zhao, Y. Sulfur-doped g-C<sub>3</sub>N<sub>4</sub>/rGO porous nanosheets for highly efficient photocatalytic degradation of refractory contaminants. *J. Mater. Sci. Technol.* **2020**, *41*, 117–126. [[CrossRef](#)]
40. Pradhan, D.; Nayak, N.; Kanar, M.; Kumar Dash, S. Effortless Fabrication of Bi<sub>2</sub>O<sub>3</sub>-Co<sub>3</sub>O<sub>4</sub> Nanocomposite Catalyst: Harnessing Photocatalytic Power for Efficient Cationic Dye Degradation. *ChemistrySelect* **2024**, *9*, e202400217. [[CrossRef](#)]
41. Liu, X.; Yang, Z.; Zhang, L. In-situ fabrication of 3D hierarchical flower-like β-Bi<sub>2</sub>O<sub>3</sub>@CoO Z-scheme heterojunction for visible-light-driven simultaneous degradation of multi-pollutants. *J. Hazard. Mater.* **2021**, *403*, 123566. [[CrossRef](#)]
42. Ma, H.; Yang, X.; Tang, X.; Cao, X.; Dai, R. Self-assembled Co-doped β-Bi<sub>2</sub>O<sub>3</sub> flower-like structure for enhanced photocatalytic antibacterial effect under visible light. *Appl. Surf. Sci.* **2022**, *572*, 151348. [[CrossRef](#)]
43. Xu, X.; Feng, X.; Wang, W.; Song, K.; Ma, D.; Zhou, Y.; Shi, J.W. Construction of II-type and Z-scheme binding structure in P-doped graphitic carbon nitride loaded with ZnO and ZnTCPP boosting photocatalytic hydrogen evolution. *J. Colloid Interface Sci.* **2023**, *651*, 669–677. [[CrossRef](#)]

44. Majeed Khan, M.A.; Siwach, R.; Kumar, S.; Ahmed, M.; Ahmed, J. Investigations on microstructure, optical, magnetic, photocatalytic, and dielectric behaviours of pure and Co-doped ZnO NPs. *J. Mater. Sci. Mater. Electron.* **2020**, *31*, 6360–6371. [[CrossRef](#)]
45. Zhang, D.; Su, C.; Yao, S.; Li, H.; Pu, X.; Geng, Y. Facile in situ chemical transformation synthesis, boosted charge separation, and increased photocatalytic activity of BiPO<sub>4</sub>/BiOCl p-n heterojunction photocatalysts under simulated sunlight irradiation. *J. Phys. Chem. Solids* **2020**, *147*, 109630. [[CrossRef](#)]
46. Tenri Ola, A.T.; Rahmat, R.; Fahri, A.N.; Heryanto, H.; Mutmainna, I.; Sesa, E.; Tahir, D. Synergistic Effect of Chitosan and Activated Carbon (AC) in Suppressing Recombination Charge of Composite Ca<sub>2</sub>Fe<sub>2</sub>O<sub>5</sub>–AC/Chitosan for High Photodegradation of Fipronil Wastewater. *J. Polym. Environ.* **2022**, *30*, 3218–3229. [[CrossRef](#)]
47. Hirashima, S.; Amimoto, T.; Iwamoto, Y.; Takeda, K. Photodegradation of the insecticide fipronil in aquatic environments: Photo-dechlorination processes and products. *Environ. Sci. Pollut. Res.* **2023**, *30*, 89877–89888. [[CrossRef](#)]
48. Mianjy, J.G.; Niknafs, B.N. Photodegradation of fipronil in natural water by high intensity UV light under laboratory conditions. *Asian J. Chem.* **2013**, *25*, 2284–2288. [[CrossRef](#)]
49. Roulová, N.; Hrdá, K.; Kašpar, M.; Peroutková, P.; Josefová, D.; Palarčík, J. Removal of Chloroacetanilide Herbicides from Water Using Heterogeneous Photocatalysis with TiO<sub>2</sub>/UV-A. *Catalysts* **2022**, *12*, 597. [[CrossRef](#)]
50. Wang, Y.; Lin, C.; Liu, X.; Ren, W.; Huang, X.; He, M.; Ouyang, W. Efficient removal of acetochlor pesticide from water using magnetic activated carbon: Adsorption performance, mechanism, and regeneration exploration. *Sci. Total. Environ.* **2021**, *778*, 146353. [[CrossRef](#)]
51. Yi-Zhu, P.; Wan-Hong, M.; Man-Ke, J.; Xiao-Rong, Z.; Johnson, D.M.; Ying-Ping, H. Comparing the degradation of acetochlor to RhB using BiOBr under visible light: A significantly different rate-catalyst dose relationship. *Appl. Catal. B Environ.* **2016**, *181*, 517–523. [[CrossRef](#)]

**Disclaimer/Publisher’s Note:** The statements, opinions and data contained in all publications are solely those of the individual author(s) and contributor(s) and not of MDPI and/or the editor(s). MDPI and/or the editor(s) disclaim responsibility for any injury to people or property resulting from any ideas, methods, instructions or products referred to in the content.